IEEE Access
Multidisciplinary ⋮ Rapid Review ⋮ Open Access Journal

Received June 13, 2020, accepted June 22, 2020, date of publication July 3, 2020, date of current version July 20, 2020.

Digital Object Identifier 10.1109/ACCESS.2020.3006875

A General Mathematical Model for LVRT Capability Assessment of DER-Penetrated Distribution Networks

POUYA SALYANI[1], KAZEM ZARE[1], MEHDI ABAPOUR[1], (Member, IEEE), AMIN SAFARI[2], AND MIADREZA SHAFIE-KHAH[3], (Senior Member, IEEE)

[1]Electrical Engineering Department, University of Tabriz, Tabriz 80309, Iran
[2]Department of Electrical Engineering, Azarbaijan Shahid Madani University, Tabriz 5375171379, Iran
[3]School of Technology and Innovations, University of Vaasa, 65200 Vaasa, Finland

Corresponding authors: Kazem Zare (kazem.zare@tabrizu.ac.ir)

The work of Miadreza Shafie-Khah was supported by the SolarX Research Project, Business Finland, 2019–2021, under Grant 6844/31/2018.

ABSTRACT Low voltage ride through (LVRT) is one of the indispensable issues of recent decade in the context of grid codes. LVRT stands for the ability of a generation facility to stay connected during the voltage dip. Despite the numerous discussions in recent works, but they mostly concentrate on the LVRT-based control of distributed energy resources (DERs) integrated into a microgrid and its improvement. However, what has been hidden and not addressed any more yet is an index to measure the LVRT capability of a DER-penetrated distribution network (DPDN) under different voltage sags. This takes precedence when we want to evaluate the LVRT capability of DPDNs with consideration of various LVRT categories of DERs mandated in IEEE 1547 standard. This paper introduces a general framework for LVRT assessment of a DPDN by solving a system of differential algebraic equations (DAEs). Then expected LVRT capability of a DPDN is evaluated by a proposed LVRT index through the implementation of Monte Carlo simulation technique.

INDEX TERMS Differential algebraic equation (DAE), distributed energy resource (DER), penetrated distribution network (DPDN), low voltage ride through (LVRT), Monte Carlo.

I. INTRODUCTION

Low voltage ride-through (LVRT) concept accounts as one of the ride-through capability of distributed energy resources (DERs) in abnormal operation conditions, considered in the power system grid codes. LVRT entails limiting the active power amount of the DER as was generated in steady state and increasing the injection of reactive power. This can help raise the voltage in the abnormal operation mode of the network and provide a situation to stay connected.

The abnormal operation mode in the distribution sector stands for a condition of a network in which voltage or frequency of network deviates from its nominal value. About the voltage, any sudden drop below the 90% of nominal value accounts as the abnormal condition and response of DERs to this short term voltage drop is known as their abnormal operating performance. This response of DER affects a limited area supplied by the main substation and helps raise the voltage to an acceptable level.

It was mandatory to immediately trip the DER in the past decades by the occurrence of a voltage drop (with any time duration of abnormal condition) on its point of common coupling (PCC). For the DER trip, there was no difference between a short-term voltage drop caused by transient events (such as transient faults) and the voltage drops with considerable time duration.

With the incoming last decade and increasing the growth of DER capacity, the power system faced with an essential problem. Sudden loss of a considerable capacity of DERs encounters the power system into the risk of blackout.

Indeed, the modern power systems supply a large number of their loads by the distributed generation that its loss may result in various kinds of instabilities in the upstream grid and

The associate editor coordinating the review of this manuscript and approving it for publication was Ahmed Aboushady.

consequently the cascading failures. Hence it was decided to equip the installed DERs to LVRT ability to keep on the DERs through the short term voltage drop of its PCC.

Various countries have their specific grid code which includes the LVRT capability of DERs too. In general, two abnormal operating performance categories are defined for the LVRT capability of DERs, category I and category II. However, the newly published IEEE standard 1547 [1], has introduced three categories (all with full explanation are given). As an example, the LVRT capability defined in German grid code [2] is shown in Fig. 1 for the two abnormal operating categories of DERs. It can be seen that the category II DERs have more chance to withstand the abnormal condition rather than the category I.

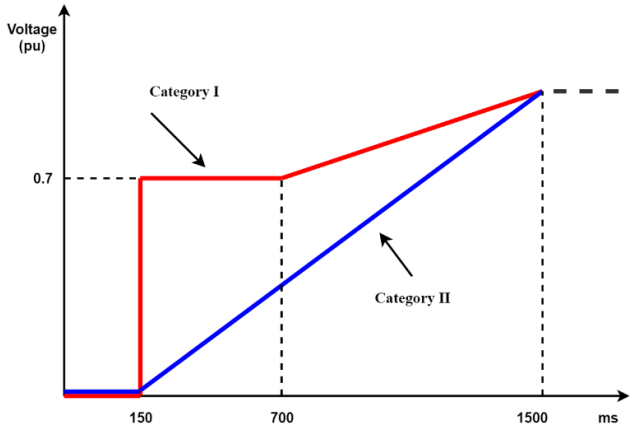

FIGURE 1. LVRT capability curve for the two types of categories.

Two border lines depicted in Figure 1 (for two LVRT performance categories) distinguish between the ride through zone and trip zone of the DER. Ride through the zone is the area above the border and trip zone includes the area below the border. Suppose an abnormal condition of network with clearing time of 400 ms that causes the drop of PCC voltage to about 60% of nominal voltage. For a category I DER which requires a PCC voltage higher than 0.7 pu, this PCC voltage has a lower value and results in operation cessation of the DER for several minutes.

While according to this figure, a category II DER can ride through this short term voltage dip and withstand during this abnormal condition. In addition, severe voltage dips in PCC voltage with a longer duration can lead to the trip of DERs with both LVRT performance categories I and II. But at all category II DERs have more chance to successfully riding through the different short term voltage dips.

In the field of DER LVRT and its improvement, numerous works have been carried out. Mainly the inverter-based DERs like photovoltaic (PV) [3]–[5] and wind turbine (WT) [6]–[8] that their control strategy to better ride through the PCC voltage dip was fully discussed. In [9], LVRT enhancement of a PV system was achieved by optimally tuning of PI control parameters of both the DC-DC converter and the grid side inverter to reach the maximum power point tracking and increase the PCC voltage. Besides, the stability analysis of DERs, such as a doubly-fed induction generator (DFIG) with consideration of LVRT was evaluated in [10] and [11]. In [12], the LVRT ability of DFIG-WTs after the occurrence of symmetrical and unsymmetrical faults has been improved by controlling the stator voltage of DFIG through its rotor side converter.

In [13] and [14], the LVRT behavior of solar generation in direction with transient analysis was evaluated in a multi-machine power system. Also, the frequency of the center of inertia to improve the LVRT and transient stability of a multi virtual synchronous generator power system has been implemented in [15].

Dynamic reactive power injection and LVRT support were addressed in [16] for a power system integrated with large scale WTs. Ref. [17] proposed a control strategy based on the mixed potential function to limit the inverter current against both the balanced and unbalanced faults and also regulate the amount of reactive power injection. Fast transition from normal operation mode to the LVRT mode accounts as another advantage of this control method.

Also, fuzzy logic controllers have represented acceptable results in the LVRT performance of inverter-based DERs. In [18], a robust Sugeno fuzzy logic controller was designed for the back to back converter of variable speed WT utilized as a permanent magnet synchronous generator (PMSG). With the help of this controller and the Wale optimization algorithm, enhancement of LVRT performance and power-tracking maximization of the WT are achieved in the bi-objective framework. For three phase PV systems, Ref. [19] implemented Takagi-Sugeno fuzzy neural network to control the reactive power injection during the LVRT mode of operation. It has used an online learning algorithm to enhance the LVRT performance of PV,considering uncertainties in the fuzzy-neural control.

For the sake of DER synchronization during the faulty condition of the network, the phase-locked loop (PLL) is implemented. Authors in [20] have proposed a low-pass notch PLL as a robust PLL,which is based on fast Fourier transform concept. Using the phase angle extracted from this PLL and with the help of LVRT current injection strategies, a feasible ride through has been guaranteed for grid-connected inverter-based DERs under balanced and unbalanced faults.

Apart from controlling methods, the role of fault current limiters in the LVRT performance of DERs is one other issue that was discussed in [21] and [22]. In [21], LVRT enhancement of an offshore wind farm was carried out through the cooperation of superconducting fault current limiters located in the feeders to suppress fault currents and alleviation of sag effect. Due to the weak cost-effectiveness of traditional superconducting fault current limiters, Ref. [22] validated the effect of resistive type superconducting fault current limiters in the LVRT improvement of PMSGs in a cost-effective manner.

Microgrid design concerning the forthcoming grid codes was pointed out in [23] and [24]. Optimally, the determination of penetration level of PVs in a distribution network and their converter size were carried out in [25]. In [26], the neural network concept was used to control and enhance the LVRT functionality of microgrids. Droop-based control method was introduced by [27] and [28] to improve the LVRT in microgrids. The LVRT behavior of microgrids by applying the consensus-based distributed control was investigated in [29]. Ref. [30] performed a dynamic LVRT analysis for a microgrid with weak grid connection from the viewpoint of stability and DER control modes.

When a fault occurs in a power system, one major issue is the current injection of inverter-based DERs. Ref. [31] has proposed a theoretical method to calculate this fault current for the PV with consideration of its DC bus fluctuations to use in the LVRT assessment. Such calculations have to consider the network topology, its parameters and the type of faults that occur within the network.

In a power system, for buses that are equipped with DER, there exists a challenge that is determining the area of vulnerability. An area of vulnerability refers to the electrical boundary in which fault occurrences affect the certain sensitive buses (either load or generation buses). Since the buses including DERs with LVRT capability are sensitive to the depth of voltage sag, Ref. [32] has addressed a new method based on bisection search, which determines the areas of fault occurrence do not trigger the LVRT performance for these DERs. However, such problems (especially in the LVRT context) may take importance in meshed high voltage power system rather than radial MV feeders.

At all, the previous works can be summarized into four contexts, devices and control methods to LVRT enhancement and performance improvement of DERs, dynamic stability of DERs with LVRT ability, synchronization of DERs during the LVRT performance and area of vulnerability for DER LVRT mode of operation. Nevertheless, what has been overlooked in these works is the LVRT performance behavior of a whole active distribution network.

To explain this point, consider a DER-penetrated distribution network (DPDN) and the DERs with different abnormal operating performance categories. There are essential factors that affect the whole LVRT capability of a DPDN, such as the size and location of DERs, the network topology of MG (number of buses and connectivity) and the DER abnormal operating performance categories. The DER size has a direct impact on the current injection amount, either active or reactive to raise the PCC voltage. The DER bus location takes on importance in large DPDNs where the DERs farther from the sag location have a higher chance of staying connected.

In addition, the voltage rise of network and PCCs depends indirectly on the network topology and the DERs abnormal operation category which is of importance and determines its ride-through ability to withstand against the voltage sags. Furthermore, the bus loads can be taken into account in the distribution sector as they can affect the PCC voltage in sag duration. These are all important factors that were not considered in previous studies. However, [33] has just addressed the penetration level impact on voltage instability of a PV-penetrated distribution network and its LVRT capability.

Furthermore, these works have not discussed the conditions of the network that cause the failure of DERs in riding through the short term voltage drop of the PCC. This failure refers to sag depth, sag duration and abnormal condition performance category of DERs. Another disregarded point is the overall DER capacity that is tripped over the abnormal mode of operation. This sudden loss of generation capacity follows the probability of any trouble in the local supplying area or even the bulk power system.

The aim of this paper is the LVRT assessment of DPDNs with an acceptable penetration level of DERs and the proposition of a general mathematical model. Moreover, an index is proposed to capture the LVRT capability of DPDN under the stochastic nature of voltage sags. Unlike the works mentioned above that focus more on the LVRT performance of a single DER in a microgrid and their control methods, this aspect of LVRT assessment helps us reach an analytical viewpoint about the performance of DPDNs under different voltage sags. Especially, to see the LVRT response of several DERs within a DPDN to different voltage sags and determining the DERs that cease to energize during the abnormal voltage condition of the network.

This viewpoint on DPDNs is of importance as it can be used in the future expansion planning of DPDNs with the orientation of LVRT enhancement. Also, for a power system with several DPDNs, blackouts as a consequence of DER trips are a significant concern and to have a general and simplified study about such blackouts, this viewpoint can be helpful.

The next section explains these two concerns and elaborates on the contribution of the paper. Section III gives the mathematical formulation of the problem and section IV discusses the solution of solving the DAE. The results are demonstrated and evaluated in section V and the conclusion is given in the last section.

II. CONTRIBUTION

Let us consider a medium voltage distribution network integrating a specific number of DERs that is so-called a DPDN. This DPDN can have different abnormal operating performance categories pertaining to the country grid code. When the network faces a short term voltage dip, the DERs which cannot meet the relevant LVRT requirement curve should cease to energize.

About the short-term voltage dips, typically known as voltage sag, there are several types of equipment in distribution networks sensitive to these anomalies. Thus the equipment has different responses to voltage sags. This response can either follow the trip of equipment or successfully riding through the voltage sag.

Authors in [34] and [35] have introduced an index for sag severity to see the equipment tolerance and a distribution network performance under different sag depth and duration. Also, they have represented a frequentist inference for the voltage sag occurrences in the distribution network. Evaluation of network performance in the presence of voltage sag was developed in [36] and [37] by considering the probabilistic viewpoint and protection device settings. The equipment trip probability is demonstrated in contour lines for different applied voltage dips. Authors have used this methodology to estimate the economic damages and reliability indices due to the interruptions caused by voltage sag in the distribution system.

Ref. [38] has modeled the tolerance curve of equipment against the voltage sags and their failure possibility in the fuzzy environment. However, voltage sag is modeled in a probabilistic environment with probability density function, which yields the evaluation of network performance in a fuzzy probabilistic manner. Ref. [39] has introduced a voltage sag impact factor with consideration of the sensitivity region for equipment. This index is applicable in the probabilistic evaluation of site performance under different voltage sags.

The Origin of voltage sags is an essential point to be discussed. The origin of sags can be within the DPDN itself (such as faults occur in equipment or motor start-up) or in the transmission sector that mostly contains the transient faults. There are several methods to detect the sag origin. In [40] as one of the recent works, a hybrid method was implemented for a distribution system to find out that the origin of voltage sags is downstream of the HV/MV substation or above. Also, it has taken into account the LVRT performance of DERs in the measurements conducted in HV/MV substations to detect the origin of faults.

Note that voltage sags originated from out of the DPDNs in the transmission sector have different impacts from those caused by faults or sudden overloading within the DPDN itself. Nevertheless, here is a key question that should be responded to. Is it necessary to consider both cases about the sag origin in our analysis?

At first, the sags originated from the inside of DPDN are considered. It is worth mentioning that the tripping of DERs, which belong to a single DPDN for several minutes, does not have any significant effect on the power system. At most, it may result in the de-energization of its local loads for a few periods. Then the loads are restored and the DPDN can proceed to its normal operation.

In contrast, when a transient fault takes place at the transmission level, it affects a large number of distribution feeders equipped with DERs. These feeders have different reactions to the voltage sags concerning the DER types and their LVRT capability.

Thus, it is possible for a large number of these DERs not to withstand the voltage sag and cease to energize. This can be enough for the power system to run into a blackout by a sudden loss of huge generation capacity at the distribution level [41]. Thus, it seems plausible to ignore the sags originated from the inside of the DPDNs and focus on the sags caused by transient faults in the transmission level.

Now when voltage sag appears on the subtransmission substation, consequently, the PCC voltage of DERs is affected. Depending on the sag level and duration and especially the LVRT categories, some of the DERs meet the LVRT requirement and stay connected. The others that cannot withstand this situation should be tripped. Therefore, it is possible for a DPDN to suddenly lose a portion of its generation. From the power system point of view, the higher the amount of lost generation in DPDNs, the higher the risk of going into instabilities and blackouts.

Therefore, the primary purpose of this paper is to first give a mathematical model based on the system of differential algebraic equations (DAEs) to see the LVRT-based behavior of a DPDN during voltage sag. This helps to find out which DERs should cease to energize under specific voltage sag. Then, the Monte Carlo simulation is carried out for different sag severities and durations to obtain the LVRT capability of DPDNs and their expected lost generation capacity.

In this study, note that it is not important to perform fault analysis in the transmission network to reach the sag behavior at the distribution level. However, what is aimed is to attain an approximate behavior from the LVRT performance of DPDNs in the presence of several DERs with different abnormal operating performance categories.

Besides, this paper studies the LVRT capability of DPDNs from the perspective of the DER category, hence it is not important to take into account the type of DERs with the same category (such as WT and PV as inverter-based DERs). These DERs have the same abnormal operation categories, albeit their different internal dynamical behavior. Nevertheless, this paper does not give importance to this difference in transient behavior of DERs and their stability issues are ignored.

Moreover, this work provides a context for future works to study the impact of DPDN LVRT behavior on the contingency analysis and blackout risk assessment in the power system. This is of importance, as evaluating the response of whole DERs in a power system to different voltage sags is a time-wasting and so complicated work. Such projects require a massive data about downstream networks and DERs.

Furthermore, this framework helps to look ahead to the expansion planning in the distribution level and sitting and sizing of DERs with consideration of LVRT. Its reason is that the existing strategies for increasing DER capacity just consider the cost and reliability issues. But for a power system that will face high penetration of DERs, the LVRT capability of its future DPDNs plays a key role.

The aforesaid expected LVRT capability is defined in an index that is discussed later. The importance of this index is discussed in section IV. Furthermore, it should be emphasized that this paper has not any concentration on the control issues of DERs and improvement of their LVRT operational, but suggests a framework to better resolve the main LVRT problems in the future works.

III. MATHEMATICAL FORMULATION

Before the explanation of the model, some assumptions must be regarded. First, the dynamic stability of the DPDN and DERs themselves are not the issue. So about the inverter-based DERs, its time-variant behavior in the ac side after the inverter is required. Also the synchronous type DERs are analyzed from the LVRT standpoint and their transient stability is not considered herein.

In addition, the load points during the sag period are assumed to be modeled as an impedance load. Two categories of DERs, synchronous and inverter-based are considered and their time-variant behavior during the transient period is given in the following.

A. SYNCHRONOUS GENERATORS

In the distribution level, this type includes mostly the diesel generators in capacity of just several megawatts. Thus it is acceptable to formulate them in a third order model [42]. Following equations represent the dynamic behavior of kth synchronous generator in dq reference frame. Equations (1)-(4) show the dynamic state of rotor angle, angular velocity, internal voltage and exciter voltage respectively and (5)-(6) relate to the stator equations of the generator.

$$\frac{d\delta_k}{dt} = \omega_{0,k}.(\omega_k - 1) \tag{1}$$

$$\frac{d\omega_k}{dt} = \frac{1}{M}\left(P_{m,k} - P_{T,k} - D_k.(\omega_k - 1)\right) \tag{2}$$

$$\frac{dE'_{q,k}}{dt} = \frac{1}{T'_{d0.k}}\left(E'_{fd,k} - E'_{q,k} + \left(x_{d,k} - x'_{d,k}\right).i_{d,k}\right) \tag{3}$$

$$\frac{dE'_{fd,k}}{dt} = -\frac{1}{TA_k}E'_{fd,k} + \frac{KA_k}{TA_k}\left(V_{ref,k} - V_{B,k}\right) \tag{4}$$

$$V_{bd,k} = x_{q,k}.i_{q,k} \tag{5}$$

$$V_{bq,k} = E'_{q,k} - x'_{d,k}.i_{d,k} \tag{6}$$

where

$$P_{T,k} = E'_{q,k}.i_{q,k} + \left(x_{q,k} - x'_{d,k}\right).i_{d,k}.i_{q,k} \tag{7}$$

$$V_{B,k} = \sqrt{V_{bd,k}^2 + V_{bq,k}^2} \tag{8}$$

The terminal electric power, bus voltages and stator currents are shown by P_T, V_{bdq} and i_{dq} respectively. The parameters P_m and V_B refer to the input mechanical power and absolute bus voltage respectively. The other parameters given in these equations such as excitation gains and time coefficients are addressed in [42].

B. INVERTER-BASED DERS

Equations for inverter-based DERs consist of two terms, one relates to the LCL filter and other relates to the controller part. The related equations for the ith DER of this type are given below.

$$\frac{di_{d,i}}{dt} = \frac{-R_{f,i}}{L_{f,i}}i_{d,i} + \omega_0.i_{q,i} + \frac{1}{L_{f,i}}\left(v_{d,i} - v_{od,i}\right) \tag{9}$$

$$\frac{di_{q,i}}{dt} = \frac{-R_{f,i}}{L_{f,i}}i_{q,i} - \omega_0.i_{d,i} + \frac{1}{L_{f,i}}\left(v_{q,i} - v_{oq,i}\right) \tag{10}$$

$$\frac{dv_{od,i}}{dt} = \omega_0.v_{oq,i} + \frac{1}{C_{f,i}}\left(i_{d,i} - i_{bd,i}\right) \tag{11}$$

$$\frac{dv_{oq,i}}{dt} = -\omega_0.v_{od,i} + \frac{1}{C_{f,i}}\left(i_{q,i} - i_{bq,i}\right) \tag{12}$$

$$\frac{di_{bd,i}}{dt} = \frac{-R_{C,i}}{L_{C,i}}i_{bd,i} + \omega_0.i_{bq,i} + \frac{1}{L_{C,i}}\left(v_{od,i} - v_{bd,i}\right) \tag{13}$$

$$\frac{di_{bq,i}}{dt} = \frac{-R_{C,i}}{L_{C,i}}i_{bq,i} - \omega_0.i_{bd,i} + \frac{1}{L_{C,i}}\left(v_{oq,i} - v_{bq,i}\right) \tag{14}$$

where $[v_{dq}, i_{dq}, v_{odq}, i_{bdq}, v_{bdq}]$ are the state variables denote to the inverter output voltage, inverter output current, capacitor voltage, bus current and bus voltage respectively. R and L are the resistance and inductance of the LCL filter and ω_0 is the base angular velocity.

These are the differential equations for the voltage and current of the inverter-based DER in dq reference frame that were fully explained in [43]. The equations related to the controller of the inverter are brought in (15)-(18) which consist of current controller equations and voltage controller equations.

$$\frac{d\Phi_{d,i}}{dt} = I_{d,i}^{ref} - i_{d,i} \tag{15}$$

$$\frac{d\Phi_{q,i}}{dt} = I_{q,i}^{ref} - i_{q,i} \tag{16}$$

$$v_{d,i}^{ref} = K_{pi}\left(I_{d,i}^{ref} - i_{d,i}\right) + K_{ii}.\Phi_{d,i} - \omega_0.L_{f,i}.i_{q,i} + V_{bd,i} \tag{17}$$

$$v_{q,i}^{ref} = K_{pi}\left(I_{q,i}^{ref} - i_{q,i}\right) + K_{ii}.\Phi_{q,i} + \omega_0.L_{f,i}.i_{d,i} + V_{bq,i} \tag{18}$$

The state variable Φ is auxiliary that helps to get rid of the integral operator in equations (17) and (18). But about the reference currents I_{dq}^{ref}, it should be noticed that they are determined at each time t according to the LVRT reactive power injection strategy given below.

$$S_{i,t} = V_{B,i,t}.I_i^N \tag{19}$$

$$Q_{i,t}^{ref} = \begin{cases} 0, & V_{B,i,t} \geq 0.9 \\ \alpha.\left(0.9 - V_{B,i,t}\right).S_{i,t}, & 0.2 \leq V_{B,i,t} < 0.9 \\ S_{i,t}, & 0 \leq V_{B,i,t} < 0.2 \end{cases} \tag{20}$$

$$P_{i,t}^{ref} = \sqrt{S_{i,t}^2 - Q_{i,t}^{ref\,2}} \tag{21}$$

$$I_{d,i,t}^{ref} = \frac{V_{bd,i,t}.P_{i,t}^{ref} + V_{bq,i,t}.Q_{i,t}^{ref}}{V_{bd,i,t}^2 + V_{bq,i,t}^2} \tag{22}$$

$$I_{q,i,t}^{ref} = \frac{V_{bq,i,t}.P_{i,t}^{ref} - V_{bd,i,t}.Q_{i,t}^{ref}}{V_{bd,i,t}^2 + V_{bq,i,t}^2} \tag{23}$$

The parameter I^N denotes the nominal current of the inverter in the abnormal operation mode of the network and S is the permissible apparent power injection in that time step. Reference active and reactive powers set in each time step are shown by $P_{i,t}^{ref}$ and $Q_{i,t}^{ref}$. The absolute bus voltage of the DER is shown by V_B and α is a coefficient with a value of about 1.43.

C. NETWORK EQUATIONS

Now we have a set of DERs with any type integrated into a DPDN that injects current during the sag period. This follows the equation of voltage-current (24) by taking into account the admittance matrix of the network. Since DPDNs usually have higher number of buses in comparison with transmission networks, it is better to reduce the size of the admittance matrix using Kron reduction method [44]. This helps in lowering the number of overall equations.

$$Y^R_{Bus}.\bar{V} = \bar{I} \tag{24}$$

In (24), Y^R_{Bus} is the reduced-size admittance matrix, $\bar{V}$ and $\bar{I}$ are the bus voltages and current injection matrices. These buses include the PCC of DERs and the substation bus. However, since the (24) has a complex form, equations (25) and (26) are extracted to simplify the modeling. In these equations, G and B are the real and imaginary parts of the admittance matrix.

$$G.\bar{V}_D - B.\bar{V}_Q = \bar{I}_D \tag{25}$$

$$B.\bar{V}_D + G.\bar{V}_Q = \bar{I}_Q \tag{26}$$

As it is seen, the voltage and currents are given in DQ axes which is the common reference frame [45]. Equation (27) gives the relationship between the two reference frames for a sample variable F, where T is the transfer function.

$$\begin{bmatrix} F_D \\ F_Q \end{bmatrix} = \begin{bmatrix} Cos\,(\delta) & \text{Sin}\,(\delta) \\ -Sin\,(\delta) & Cos\,(\delta) \end{bmatrix} . \begin{bmatrix} F_d \\ F_q \end{bmatrix} = T . \begin{bmatrix} F_d \\ F_q \end{bmatrix} \tag{27}$$

So by redefining the transfer function T in diagonal form, the voltage-current equations can be rewritten as follows. Matrix $\boldsymbol{\Upsilon}$ is the modified form of the reduced admittance matrix.

$$\begin{bmatrix} G & -B \\ B & G \end{bmatrix} .T. \begin{bmatrix} \bar{V}_d \\ \bar{V}_q \end{bmatrix} = T . \begin{bmatrix} \bar{I}_d \\ \bar{I}_q \end{bmatrix} \tag{28}$$

$$T^{-1} . \begin{bmatrix} G & -B \\ B & G \end{bmatrix} .T. \begin{bmatrix} \bar{V}_d \\ \bar{V}_q \end{bmatrix} = \boldsymbol{\Upsilon} . \begin{bmatrix} \bar{V}_d \\ \bar{V}_q \end{bmatrix} = \begin{bmatrix} \bar{I}_d \\ \bar{I}_q \end{bmatrix} \tag{29}$$

IV. DAE AND LVRT CAPABILITY ASSESSMENT

A. DAE SOLVE APPROACH

By taking a look at the aforementioned equations, it can be seen that some of them are differential equations and the others are algebraic equations that can be modeled in a form like (30). This is a nonlinear system of semi-explicit DAE [46], constructed of differential and algebraic terms. The differential variables are shown by vector $\mathbf{x}$, the algebraic variables are shown by vector $\mathbf{z}$ and $\mathbf{u}_t$ is the time-dependent vector of input parameters.

$$\begin{cases} \dfrac{d\mathbf{x}}{dt} = \mathbf{f}\,(\mathbf{x}, \mathbf{z}, \mathbf{u}_t, t) \\ 0 \quad = \mathbf{g}\,(\mathbf{x}, \mathbf{z}, \mathbf{u}_t, t) \end{cases} \tag{30}$$

There exist several methods to solve the DAE problems that the well-known one is the simultaneous approach [47], [48]. In this approach, the differential equations are converted into algebraic equations at each time step h by implementation of implicit methods such as trapezoidal or backward differential formula (BDF). Using the trapezoidal method in this initial value problem, equation (30) is reformulated as (31). Index n denotes the number of time steps.

$$\begin{cases} \mathbf{x}_{n+1} = \mathbf{x}_n + \dfrac{h}{2}.\,[\mathbf{f}\,(\mathbf{x}_{n+1}, \mathbf{z}_{n+1}, \mathbf{u}_{n+1}, t) \\ \qquad\qquad +\mathbf{f}\,(\mathbf{x}_n, \mathbf{z}_n, \mathbf{u}_n, t)] \\ 0 = \mathbf{g}\,(\mathbf{x}_{n+1}, \mathbf{z}_{n+1}, \mathbf{u}_n, t) \end{cases} \tag{31}$$

Then by applying the Jacobian method to linearizing the equations in each time step, the overall DAE problem can be modeled in a general algorithm given in (32).

In (32), $\boldsymbol{\Lambda}$ is the matrix of coefficients, $\boldsymbol{\Psi}$ is the matrix of differential and algebraic variables and $\boldsymbol{\Gamma}$ denotes the output vector dependent on vectors $\mathbf{x}_n$ and $\mathbf{z}_n$. N_{TS} is the total number of time steps. At each time step, the mentioned linear system of algebraic equations is solved which is dependent on DER number set $\boldsymbol{\Theta}$.

Ξ is a function of PCC voltages and time which checks in each time step n that whether the DER number i meets the LVRT requirement or not. The output of this function is 0, unless the DER keeps its PCC voltage in acceptable level and satisfies the LVRT requirement.

$$\begin{aligned} &\{for\ n = 1 : N_{TS} \\ &\quad t_n = t_{n-1} + h \\ &\quad\ \boldsymbol{\Lambda}_{\boldsymbol{\Theta},n}.\boldsymbol{\Psi}_{\boldsymbol{\Theta},n+1} = \boldsymbol{\Gamma}_{\boldsymbol{\Theta},n} \\ &\quad \{for\ k = 1 : |\boldsymbol{\Theta}| \\ &\quad\ i = \boldsymbol{\Theta}\,\{k\} \\ &\quad\quad \{if\ \ \Xi\left(\bar{V}_{B,i,t}, t\right) == 0 \\ &\quad\quad\ J = \{J, k\} \\ &\quad\quad\ \} \\ &\quad\ \boldsymbol{\Theta}\,\{J\} = [] \\ &\quad\ \} \\ &\} \end{aligned} \tag{32}$$

where,

$$\boldsymbol{\Lambda} = \begin{bmatrix} \dfrac{\partial \mathbf{f}}{\partial \mathbf{x}} & \dfrac{\partial \mathbf{f}}{\partial \mathbf{z}} \\ \dfrac{\partial \mathbf{g}}{\partial \mathbf{x}} & \dfrac{\partial \mathbf{g}}{\partial \mathbf{z}} \end{bmatrix}, \quad \boldsymbol{\Psi} = \begin{bmatrix} \mathbf{x} \\ \mathbf{z} \end{bmatrix} \tag{33}$$

When any DER is unable to meet the LVRT requirement in time t, its relevant equations are omitted except the ones that are in relation with voltage-current equations (by setting its injected current to zero). In other words, just the nodal dq voltages of this DER as the algebraic variables remain included in the system of algebraic equations. This omission is performed with respect to the updated set Θ, So to solve the equation, matrix Λ and vector Γ are reinstructed. Also $|\Theta|$ denotes the cardinality of DER number set Θ.

Therefore, in each time step, there exists a linear system of algebraic equations that are solved to obtain the variables of the next time step, considering that it is probable to have

a reduction in the size of the equations. This reduction is due to the trip of DERs that are not able to successfully meet the LVRT requirement and shall be tripped.

B. EXPECTED LVRT CAPABILITY OF DPDN

Now it is the turn of LVRT capability assessment of the DPDN by introducing an index named ELC. ELC is the abbreviation of expected LVRT capability of a DPDN expressed in percentage and refers to the expected amount of generation capacity to remain connected during the sag period.

What is important here is that the voltage sags appear on the sub-transmission substation have stochastic nature, whether its severity or its duration. Hence these parameters can be taken into account as a random variable.

Monte Carlo simulation is an effective way to model the stochastic behavior of voltage sags for both the sag severity ϑ and the duration τ. It can help to observe most of the possible outcomes and lets you have a better and more accurate perspective about the LVRT behavior of DPDN under abnormal conditions. To this end, the associated random variables are generated in NS number of scenarios based on the maximum sag level of V_{sag} and the maximum sag duration of T_{sag}.

The ELC index for a DPDN is defined in (34). In this formula, $\mathbf{\Omega}_D$ is the set of DER numbers, C_j is the capacity of DER j and s denotes the scenario index. $\zeta_{j,s}(\vartheta_s, \tau_s)$ is a binary variable as a function of sag level and duration, which is equal to 1 for each DER if the LVRT requirement is met. Also TDE is the total DER capacity of the DPDN calculated in (35).

$$ELC = \frac{1}{NS} \frac{\sum_{s=1}^{NS} \sum_{j \in \Omega_D} \zeta_{j,s}(\vartheta_s, \tau_s) C_j}{TDE} \times 100\% \quad (34)$$

$$TDE = \sum_{j \in \Omega_D} C_j \quad (35)$$

As the ELC index percentage is higher, it states that the DPDN is more resilient to the voltage sags from the LVRT standpoint. The ELC of 1 indicates that all the DERs within the DPDN proceed to operate and the ELC of 0 stands for tripping of all the DERs for any kind of sags. In other words, with ELC close to 1, it is so probable for DERs to stay connected in any abnormal operating condition.

While for ELC close to 0, the DPDN has a little chance to withstand the sags from the LVRT aspect and loses its DER capacity. To explicate the importance of the work from another aspect, consider a schematic of power system under high penetration of DERs depicted in Fig. 2.

The system is exposed to the risk of blackouts due to an unexpected trip of a large portion of generation in the DPDNs in the case of short term faults occurrence in the transmission sector and this is a concerning issue for the transmission system operators (TSO).

TSO usually has great knowledge about the transmission sector, its operation and dynamic behavior but does not have a better and clear view on the distribution level. Furthermore, the TSO has no analytic perspective about the effect of a sudden loss of several Gigawatts of capacity on the whole system due to the transient fault occurrence.

Hence by extracting the ELC index value for each distribution feeder, it can give a broad view about the system LVRT functioning to the TSO to better cope with this problem and alleviate the difficulties after such abnormal conditions. This index captures the LVRT strength of all the DPDNs in a power system. Thus it may be necessary for the DPDNs with lower capability of LVRT to place some additional DERs with high LVRT capability or replace the low category DERs with higher LVRT category DERs.

To have a survey of the aforesaid discussion, a flowchart is given in Fig. 3 which pictures the overall progress of LVRT assessment in a DPDN.

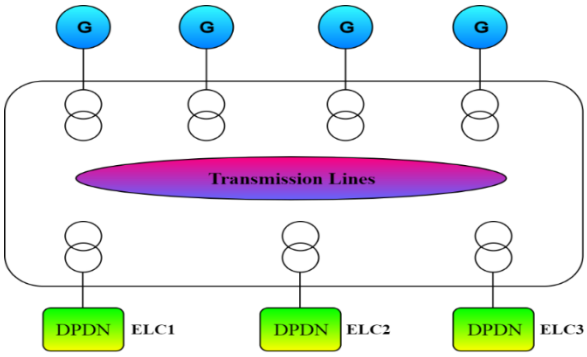

FIGURE 2. Schematic of a general power system.

TABLE 1. Required data about DERS existing in the DPDN.

DER Number	DER category	DER size (kW)	DER location
1	2	1000	3
2	2	900	14
3	1	1300	29

V. TEST NETWORK AND SIMULATION RESULTS

To verify the validity of the proposed framework, the IEEE 33 bus standard test system [49] shown in Fig. 4, is chosen as the DPDN, and three case studies are considered. At all just two types of DERs are taken into account as the installed units in this network; diesel engine generator as synchronous and WT as inverter-based generators, and the other types are not used. The required data about the diesel generator and the WT to solve the problem can be found in [50] and [51], respectively.

A. STUDY CASE I

In the first study case, the represented mathematical model is verified and the LVRT behavior of a DPDN with the penetration level of about 70% is analyzed. Three DERs are used in this DPDN and Table 1 shows the organization of these DERs.

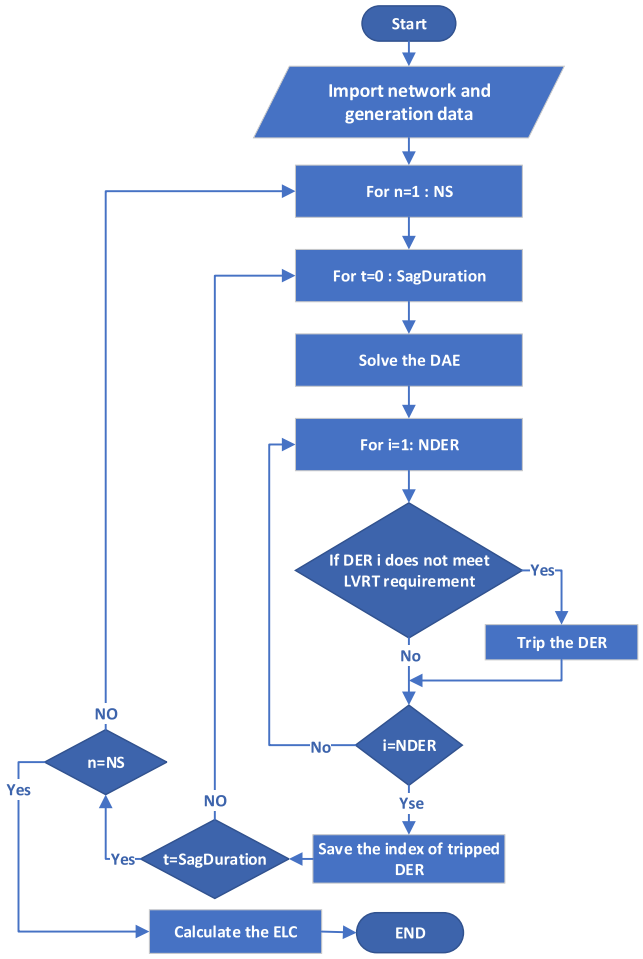

FIGURE 3. Flowchart of LVRT assessment progress.

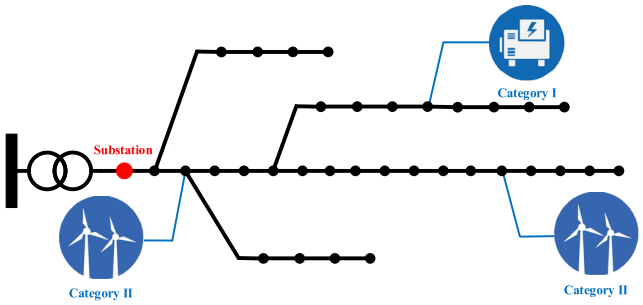

FIGURE 4. Schematic view of a DPDN.

Fig. 5 depicts the voltage variation of the buses connected to the DERs for a voltage sag of 90% and a clearing time of about 800 ms. This voltage reduction percentage is applied to the DPDN substation.

In the absence of DERs, the voltage of the network buses would drop to about 0.1 pu, but with the help of LVRT facility, the dynamic voltage profile is changed. At first, what is seen is that all three DERs have tripped before the end of abnormal status, but what is notable is voltage changes in the PCCs.

The third DER with abnormal operating performance category of I is on for 150 ms, but is tripped due to inability to meet its relevant LVRT requirement. The category II DER

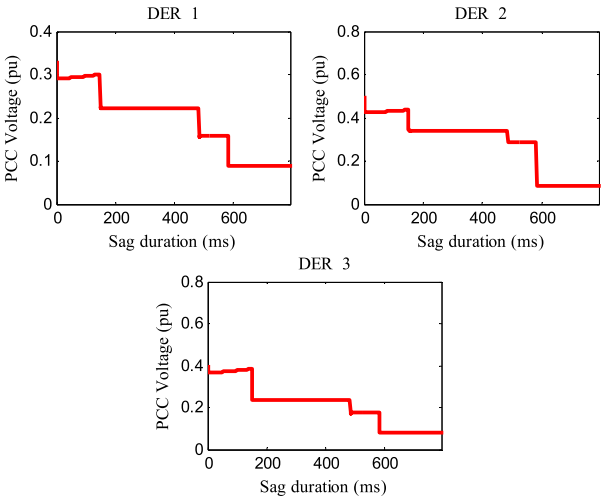

FIGURE 5. PCC voltage of DERs during the abnormal condition of network for sag level of 90% and sag duration of 800 ms.

located at bus 3 is tripped after about 530 ms. The second DER withstands the voltage sag for about 600 ms but its PCC voltage does not match the level that LVRT operation function requires and is ceases to energize.

The main reason for the first DER trip before the second one is its closer location to the HV/MV substation. DER 1 has a higher capacity, which directly affects the amount of reactive power contribution. But due to the high depth of sag and also the closer electrical distance to the substation, further increase in its PCC voltage is not possible. However, it should be noted that this injection of reactive power can affect the voltage of other buses.

The other simulation is performed for two sag severities of 70% and 50% and the sag duration of about 800 ms and 500 ms. The results are shown in Fig. 6 and Fig. 7.

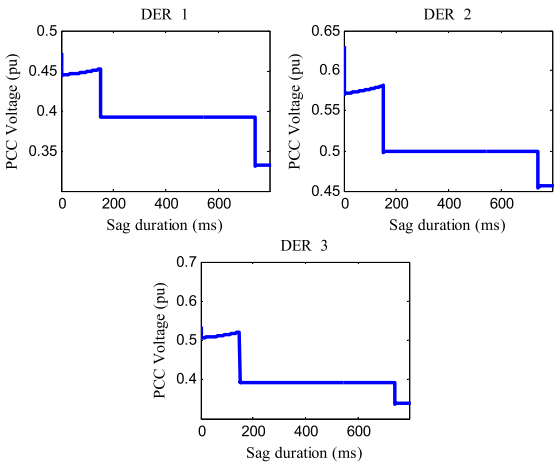

FIGURE 6. PCC voltage of DERs during the abnormal condition of network for sag level of 30% and sag duration of 280 ms.

As is seen in Fig. 6, just two DERs are tripped, unlike the previous sage level that all were tripped. By reactive power injection and with respect to the internal voltage of diesel

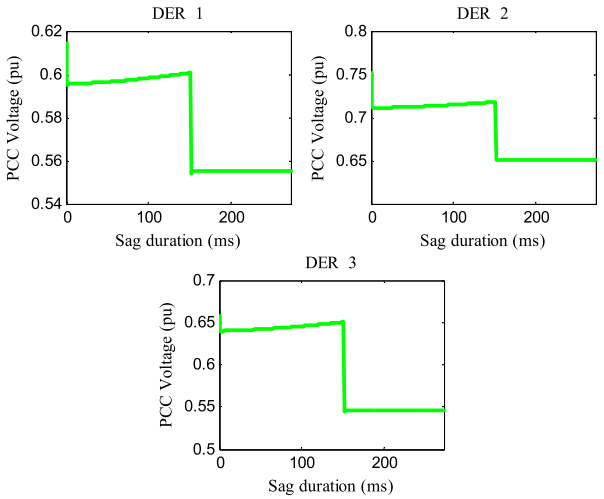

FIGURE 7. PCC voltage of DERs during the abnormal condition of network for sag level of 70% and sag duration of 280 ms.

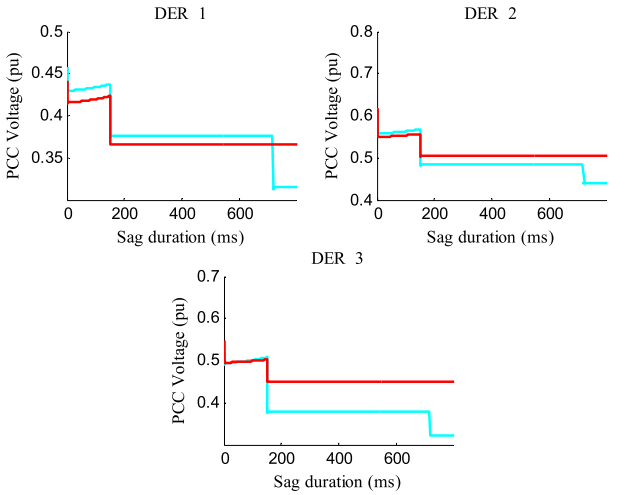

FIGURE 8. Comparison of PCC voltage for different DER allocations in sag level of 72% and sag duration of 800 ms.

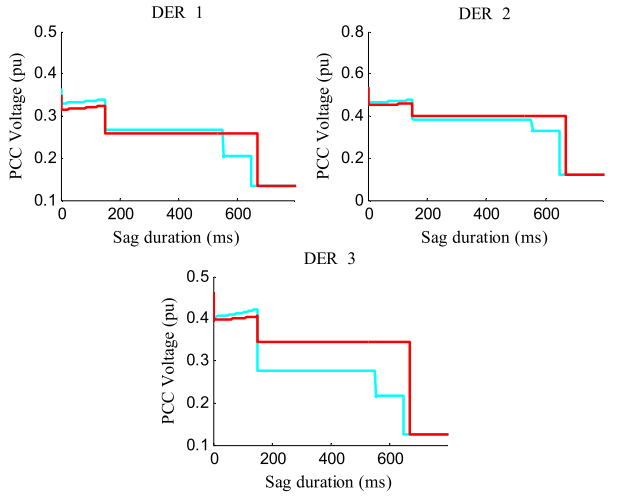

FIGURE 9. Comparison of PCC voltage for different DER allocations in sag level of 72% and sag duration of 800 ms.

engine generator, the voltage starts to rise in PCC of third DER up to the 0.52 pu. But since its PCC voltage is less than 0.70 pu, this DER ceases to energize after 150 ms. The sag duration of 800 ms does not permit the first DER to remain connected and is tripped after 739 ms because of its PCC voltage. However, the PCC voltage of the esecond DER during the abnormal period is in a manner that satisfies the LVRT requirement and stays connected.

In Fig. 7, despite the voltage rise in PCC voltage of the second DER, but PCC voltage of the third DER does not reach the acceptable level after 150 ms and shall be tripped. Concerning to the sag duration and higher LVRT capability of category II DERs compared with category I types, the two DERs are successful in meeting the LVRT requirement and have not been tripped.

To capture the impact of DERs location on LVRT behavior of DPDN, bus location of the DER 1 is replaced with bus location of the DER 3. With respect to Fig. 8, The plot shown with cyan color refers to the primary allocation of DERs and the plot with red color shows the voltage variation of PCCs in the case of replacement.

It can be observed that by replacement of DER locations, the LVRT capability of the DPDN is improved and just one DER is tripped. Its reason is that in the primary arrangement of DERs, the first DER with abnormal operation category of II is electrically close to the substation (sag location). This effects the LVRT operation of this DER, since it has limited capability of reactive power injection rather than the second DER. However, in the second arrangement, this category II DER is placed in a farther location from MV substation resulting in a successful ride through.

Also, Fig. 9 represents this comparison for sag level of 80% and duration of 800 ms. Again it can be seen that all the DERs are disconnected in the primary arrangement while in the second one, two DERs are tripped, which verifies claim of LVRT capability enhancement for DPDN.

DER capacity has its own impact on the LVRT operation of DPDN. By fixing the bus locations according to Table 1 and redefining new DER capacities {1500, 1000, 700} kW, the PCC voltages are compared in Fig. 10 during the sag period. The depth of the appeared sag is 56% and its duration is about 300 ms.

Blue and pink colors, respectively show the results of primary capacities and newly defined capacities. Increasing the capacity especially the category II DERs yields a higher amount of reactive power injection, leading to an increase in PCC voltage.

Also, the impact of the DER number increase on the LVRT operation of DERs is evaluated in this case study. Table 2 gives the related data of four DERs with their size and location.

The total DER capacity of DPDN is kept unchanged for the aforementioned primary arrangement. Fig. 11 represents the

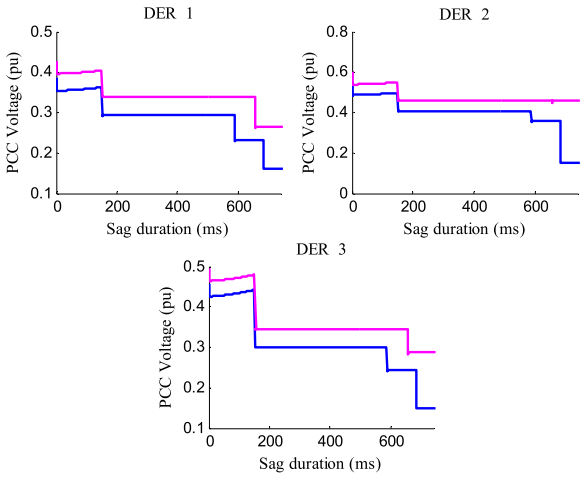

FIGURE 10. Comparison of PCC voltage for different DER capacities in sag level of 56% and sag duration of 300 ms.

TABLE 2. Required data about size, location and category of 4 DERS existing in the DPDN.

DER Number	DER category	DER size (kW)	DER location
1	2	500	4
2	1	500	13
3	2	900	23
4	1	1300	30

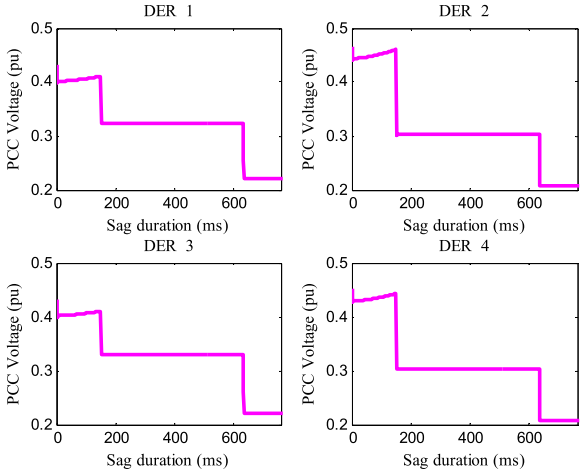

FIGURE 11. LVRT behavior of DPDN with 4 DERs in sag level of 75% and sag duration of 785 ms.

LVRT behavior of this DPDN in the sag level of 75% and sag duration of 785 ms.

The two category I DERs at buses 13 and 30 are ceased to energize after 150 ms. The other two remaining DERs at buses 4 and 23 are tripped after 636 ms and 637 ms, respectively. Nevertheless, the overall capacity of DPDN remains equal, but because a considerable percentage of this value relates to the two category I DERs, all are tripped before returning to the normal operation mode of DPDN.

So this can be concluded as an important point that an increase in the number of installed DERs does not necessarily entail the enhancement in LVRT behavior of DPDN.

B. CASE STUDY II

In the second study case, the LVRT capability assessment of the whole aforementioned primary DPDN is carried out. A Monte Carlo simulation is implemented based on the available data in Table 3 to obtain the ELC index of the DPDN. In this table, the total number of generated scenarios, lower bound and upper bound for the random variables, voltage sag severity level and sag duration are given.

TABLE 3. Required data for performing the Monte Carlo simulation.

NS	Min sag level (%)	Max sag level (%)	Min sag duration (ms)	Max sag duration (ms)
1000	15	98	50	800

The ELC value attained by applying the Monte Carlo simulation is about 0.5705. This number means that from the whole DER capacity of 3200 kW in the DPDN, just about the 57% is expected to successfully stay connected at all. To more clarify, it is expected for this DPDN among all other distribution feeders of the system to keep on 57% of its capacity in a short term abnormal condition. In other words, TSO should just rely on 57% of this DPDN capacity especially in the peak hours of the day and plan on about 43% lost generation from this capacity.

Now, if an inverter-based generator as category II is replaced with the diesel generator, it can be observed that the ELC of 0.954 is reached. This value is greater than the one obtained in the previous case and the reason definitely is the higher LVRT capability of category II DERs rather than category I DERs.

Next, the relationship between the ELC of a DPDN and the penetration level of DERs is evaluated. In this case, it is possible to observe the variation of ELC index versus the penetration level of the DPDN, which is demonstrated in Fig. 12.

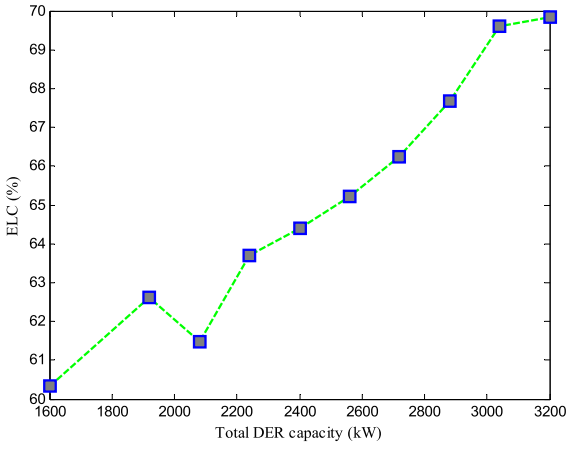

FIGURE 12. ELC variation with respect to penetration level of DERs.

The penetration level is indirectly taken with the total DER capacity of DPDN. This curve has an ascending manner at all, which means that the LVRT capability of DPDNs has almost a direct relationship with the penetration level of category II DERs.

C. CASE STUDY III

In the last study case, the LVRT behavior of DERs and the LVRT capability assessment of IEEE 69 test system [52] is conducted. The system schematic is shown in Fig. 13.

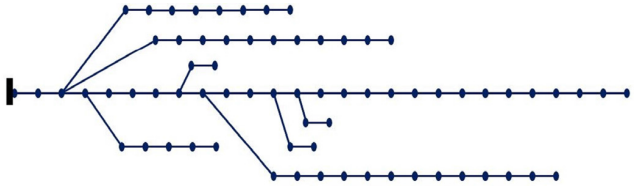

FIGURE 13. Schematic of IEEE 69 bus test system.

Table 4 provides the required data about the DERs. Four DERs are implemented to study the LVRT operation of designed DPDN, three of them with category II and one of them with category I abnormal operation capability.

TABLE 4. Required data about size, location and category of 4 DERS installed in 69 bus DPDN.

DER Number	DER category	DER size (kW)	DER location
1	2	600	4
2	2	500	16
3	1	1000	34
4	2	1000	62

Fig. 14 represents the LVRT response of DERs to a sag depth of 83% with duration of 740 ms. Since the third DER has abnormal operating performance category of I and its PCC voltage should rise to above 0.70 pu after 150 ms, it cannot meet this requirement and is tripped. Other 3 DERs

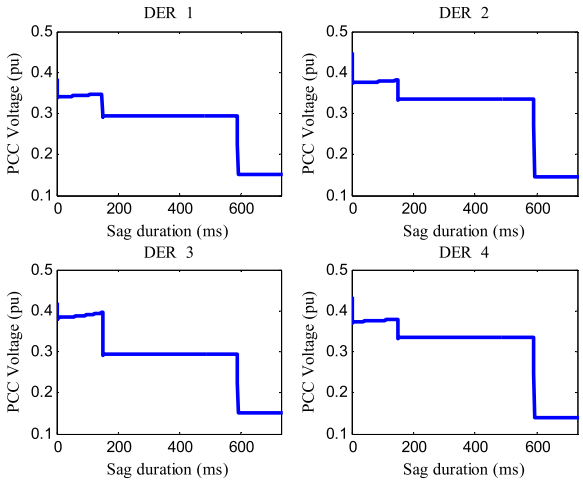

FIGURE 14. PCC voltages for sag level of 83% and duration of 740 ms.

are ceased to energize in close times 591 ms and 520 ms. This result expresses that the network has an electrical structure that makes it difficult to distinguish between the LVRT operation of DERs. While the DER located at bus 62 has a capacity of 1000 kW, but there is not any considerable difference between its PCC voltage variation and the other ones.

Fig. 15 depicts a scattered plot from the LVRT behavior of this DPDN, which shows the total lost DER capacity of DPDN for a large sample of sag level and sag duration.

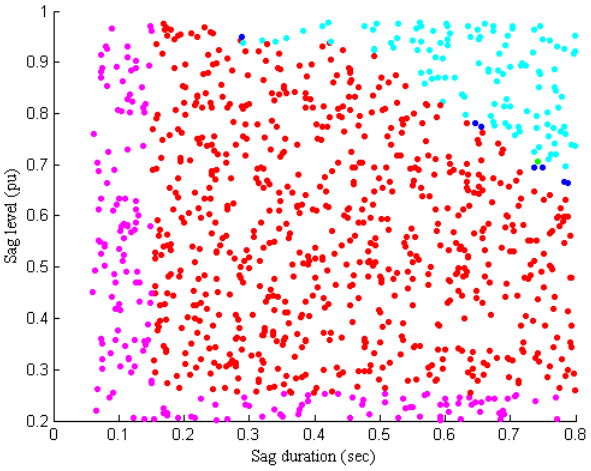

FIGURE 15. Scattered plot of total lost capacity for 69 bus DPDN.

As is seen, five colors are represented, which stand for different levels of lost capacity. The points colored with magenta indicate the contour that there is not any lost capacity. This is true as either lower sag level or sag duration increases the chance of keeping the DERs connected. Red color denotes the loss of 1000 kW that points out the trip of category I DER. Blue points stand for loss of 1600 kW capacity and green colored points, which are few denote the total capacity loss of 2600 kW. Contour colored with cyan points out the loss of whole DER capacity takes place in voltage sags with high severities and longer durations.

VI. CONCLUSION

The authors in this paper followed two main purposes. The first one was to put together a general model for the LVRT analysis of the DPDNs. This was achieved by representing a system of DAEs consisting of equations for category I DERs, category II DERs and the equations for network voltage-current relationship. As it was observed, the injection of reactive power by DERs was a compelling factor for raising the voltage of PCCs. However, the essential one was the abnormal operating performance category of DERs. Due to the lower LVRT capability of category I DERs, the short time voltage drops, especially lower than 150 ms provides an opportunity for DER to stay connected.

The second one was the assessment of LVRT capability for DPDNs using the Monte Carlo simulation. The ELC index

proposed was highly dependent on the LVRT category of DERs, which means that increasing the percentage of capacity of DERs with abnormal operating performance category of I, most probably decreases the ELC of the DPDN. Also, it was denoted that the penetration level of DERs had a positive effect on the ELC index of the DPDN. The LVRT assessment of the DPDN was carried out just under two abnormal operating performance categories of DERs and category III, which gives higher permissible stay time was not considered. This work can be a background to future studies in the LVRT-based planning of distribution networks and the effect of LVRT behavior of DPDNs on the blackouts occurring in the transmission level.

REFERENCES

[1] *IEEE Standard for Interconnection and Interoperability of Distributed Energy Resources with Associated Electric Power Systems Interfaces*, IEEE Standard 1547, 2018.
[2] Grid Code. (Apr. 2006). *High and Extra High Voltage*, E.ON Netz. [Online]. Available: http://www.eon-netz.com
[3] H. M. Hasanien, "An adaptive control strategy for low voltage ride through capability enhancement of grid-connected photovoltaic power plants," *IEEE Trans. Power Syst.*, vol. 31, no. 4, pp. 3230–3237, Jul. 2016.
[4] A. Mojallal and S. Lotfifard, "Reactive power injection strategies for single-phase photovoltaic systems considering grid requirements," *IEEE Trans. Smart Grid*, vol. 10, no. 1, pp. 546–555, Jan. 2019.
[5] F.-J. Lin, K.-H. Tan, W.-C. Luo, and G.-D. Xiao, "Improved LVRT performance of PV power plant using recurrent wavelet fuzzy neural network control for weak grid conditions," *IEEE Access*, vol. 8, pp. 69346–69358, 2020.
[6] Y. Chang, J. Hu, W. Tang, and G. Song, "Fault current analysis of Type-3 WTs considering sequential switching of internal control and protection circuits in multi time scales during LVRT," *IEEE Trans. Power Syst.*, vol. 33, no. 6, pp. 6894–6903, Nov. 2018.
[7] R. A. J. Amalorpavaraj, P. Kaliannan, S. Padmanaban, U. Subramaniam, and V. K. Ramachandaramurthy, "Improved fault ride through capability in DFIG based wind turbines using dynamic voltage restorer with combined feed-forward and feed-back control," *IEEE Access*, vol. 5, pp. 20494–20503, 2017.
[8] O. P. Mahela, N. Gupta, M. Khosravy, and N. Patel, "Comprehensive overview of low voltage ride through methods of grid integrated wind generator," *IEEE Access*, vol. 7, pp. 99299–99326, 2019.
[9] O. S. Elazab, M. Debouza, H. M. Hasanien, S. M. Muyeen, and A. Al-Durra, "Salp swarm algorithm-based optimal control scheme for LVRT capability improvement of grid-connected photovoltaic power plants: Design and experimental validation," *IET Renew. Power Gener.*, vol. 14, no. 4, pp. 591–599, Mar. 2020.
[10] R. Liu, J. Yao, X. Wang, P. Sun, J. Pei, and J. Hu, "Dynamic stability analysis and improved LVRT schemes of DFIG-based wind turbines during a symmetrical fault in a weak grid," *IEEE Trans. Power Electron.*, vol. 35, no. 1, pp. 303–318, Jan. 2020.
[11] J. Liu, W. Yao, J. Fang, J. Wen, and S. Cheng, "Stability analysis and energy storage-based solution of wind farm during low voltage ride through," *Int. J. Electr. Power Energy Syst.*, vol. 101, pp. 75–84, Oct. 2018.
[12] N. Jabbour, E. Tsioumas, C. Mademlis, and E. Solomin, "A highly effective Fault-Ride-Through strategy for a wind energy conversion system with a doubly fed induction generator," *IEEE Trans. Power Electron.*, vol. 35, no. 8, pp. 8154–8164, Aug. 2020.
[13] K. Kawabe and K. Tanaka, "Impact of dynamic behavior of photovoltaic power generation systems on short-term voltage stability," *IEEE Trans. Power Syst.*, vol. 30, no. 6, pp. 3416–3424, Nov. 2015.
[14] G. Lammert, D. Premm, L. D. P. Ospina, J. C. Boemer, M. Braun, and T. Van Cutsem, "Control of photovoltaic systems for enhanced short-term voltage stability and recovery," *IEEE Trans. Energy Convers.*, vol. 34, no. 1, pp. 243–254, Mar. 2019.
[15] M. Choopani, S. H. Hosseinian, and B. Vahidi, "New transient stability and LVRT improvement of multi-VSG grids using the frequency of the center of inertia," *IEEE Trans. Power Syst.*, vol. 35, no. 1, pp. 527–538, Jan. 2020.
[16] Z. H. Rather, Z. Chen, P. Thogersen, and P. Lund, "Dynamic reactive power compensation of large-scale wind integrated power system," *IEEE Trans. Power Syst.*, vol. 30, no. 5, pp. 2516–2526, Sep. 2015.
[17] H. Wen and M. Fazeli, "A low-voltage ride-through strategy using mixed potential function for three-phase grid-connected PV systems," *Electr. Power Syst. Res.*, vol. 173, pp. 271–280, Aug. 2019.
[18] M. H. Qais, H. M. Hasanien, and S. Alghuwainem, "Whale optimization algorithm-based sugeno fuzzy logic controller for fault ride-through improvement of grid-connected variable speed wind generators," *Eng. Appl. Artif. Intell.*, vol. 87, Jan. 2020, Art. no. 103328.
[19] F.-J. Lin, K.-C. Lu, T.-H. Ke, B.-H. Yang, and Y.-R. Chang, "Reactive power control of three-phase grid-connected PV system during grid faults using Takagi–Sugeno–Kang probabilistic fuzzy neural network control," *IEEE Trans. Ind. Electron.*, vol. 62, no. 9, pp. 5516–5528, Sep. 2015.
[20] D. Shin, K.-J. Lee, J.-P. Lee, D.-W. Yoo, and H.-J. Kim, "Implementation of fault ride-through techniques of grid-connected inverter for distributed energy resources with adaptive low-pass notch PLL," *IEEE Trans. Power Electron.*, vol. 30, no. 5, pp. 2859–2871, May 2015.
[21] H.-J. Lee, S.-H. Lim, and J.-C. Kim, "Application of a superconducting fault current limiter to enhance the low-voltage ride-through capability of wind turbine generators," *Energies*, vol. 12, no. 8, p. 1478, Apr. 2019.
[22] C. Huang, Z. Zheng, X. Xiao, and X. Chen, "Enhancing low-voltage ride-through capability of PMSG based on cost-effective fault current limiter and modified WTG control," *Electr. Power Syst. Res.*, vol. 185, Aug. 2020, Art. no. 106358.
[23] G. J. Kish and P. W. Lehn, "Microgrid design considerations for next generation grid codes," in *Proc. IEEE Power Energy Soc. Gen. Meeting*, Jul. 2012, pp. 1–8.
[24] J. Rodrigues, A. Lopes, L. Miranda, C. Gouveia, C. Moreira, and J. P. Lopes, "The role of Low-Voltage-Ride-Through capability of distributed energy resources for the mitigation of voltage sags in low voltage distribution grids," in *Proc. Power Syst. Comput. Conf. (PSCC)*, Jun. 2018, pp. 1–7.
[25] I. I. Perpinias, E. C. Tatakis, and N. P. Papanikolaou, "Optimum design of low-voltage distributed photovoltaic systems oriented to enhanced fault ride through capability," *IET Gener., Transmiss. Distrib.*, vol. 9, no. 10, pp. 903–910, Jul. 2015.
[26] L. Djilali, E. N. Sanchez, F. Ornelas-Tellez, A. Avalos, and M. Belkheiri, "Improving microgrid low-voltage ride-through capacity using neural control," *IEEE Syst. J.*, vol. 14, no. 2, pp. 2825–2836, Jun. 2020.
[27] I. Sadeghkhani, M. E. Hamedani Golshan, A. Mehrizi-Sani, and J. M. Guerrero, "Low-voltage ride-through of a droop-based three-phase four-wire grid-connected microgrid," *IET Gener., Transmiss. Distrib.*, vol. 12, no. 8, pp. 1906–1914, Apr. 2018.
[28] S. Rajamand, A. Ketabi, and A. Zahedi, "A new LVRT strategy for DGs with different droop gains in islanded microgrid with various loads," *EPE J.*, vol. 28, no. 3, pp. 116–127, Mar. 2018.
[29] W. Lee, T. Nguyen, H. Yoo, and H. Kim, "Low-voltage ride-through operation of grid-connected microgrid using consensus-based distributed control," *Energies*, vol. 11, no. 11, p. 2867, Oct. 2018.
[30] S. Mortazavian and Y. A.-R.-I. Mohamed, "Dynamic analysis and improved LVRT performance of multiple DG units equipped with grid-support functions under unbalanced faults and weak grid conditions," *IEEE Trans. Power Electron.*, vol. 33, no. 10, pp. 9017–9032, Oct. 2018.
[31] H. Liu, K. Xu, Z. Zhang, W. Liu, and J. Ao, "Research on theoretical calculation methods of photovoltaic power short-circuit current and influencing factors of its fault characteristics," *Energies*, vol. 12, no. 2, p. 316, Jan. 2019.
[32] S. Shakeri, S. Esmaeili, and M. H. Rezaeian Koochi, "Determining accurate area of vulnerability for reliable voltage sag assessment considering wind turbine ride-through capability," *Int. J. Electr. Power Energy Syst.*, vol. 119, Jul. 2020, Art. no. 105875.
[33] M. Islam, N. Mithulananthan, and M. J. Hossain, "Dynamic voltage support by TL-PV systems to mitigate short-term voltage instability in residential DN," *IEEE Trans. Power Syst.*, vol. 33, no. 4, pp. 4360–4370, Jul. 2018.
[34] H. Liao, S. Abdelrahman, Y. Guo, and J. V. Milanović, "Identification of weak areas of power network based on exposure to voltage sags—Part I: Development of sag severity index for single-event characterization," *IEEE Trans. Power Del.*, vol. 30, no. 6, pp. 2392–2400, Dec. 2015.
[35] H. Liao, S. Abdelrahman, Y. Guo, and J. V. Milanović, "Identification of weak areas of network based on exposure to voltage sags—Part II: Assessment of network performance using sag severity index," *IEEE Trans. Power Del.*, vol. 30, no. 6, pp. 2401–2409, Dec. 2015.

[36] J. C. Cebrian, N. Kagan, and J. V. Milanović, "Probabilistic estimation of distribution network performance with respect to voltage sags and interruptions considering network protection setting—Part I: The methodology," *IEEE Trans. Power Del.*, vol. 33, no. 1, pp. 42–51, Feb. 2018.
[37] J. C. Cebrian, J. V. Milanovic, and N. Kagan, "Probabilistic assessment of financial losses in distribution network due to fault-induced process interruptions considering process immunity time," *IEEE Trans. Power Del.*, vol. 30, no. 3, pp. 1478–1486, Jun. 2015.
[38] C. Behera, G. H. Reddy, P. Chakrapani, A. K. Goswami, C. P. Gupta, and G. K. Singh, "Assessment of equipment trip probability due to voltage sags based on fuzzy possibility distribution function," *IEEE Access*, vol. 6, pp. 76889–76899, 2018.
[39] M. V. Costa, J. M. C. Filho, R. C. Leborgne, and N. B. Pereira, "A novel methodology for determining the voltage sag impact factor," *Electr. Power Syst. Res.*, vol. 174, Sep. 2019, Art. no. 105865.
[40] C. Noce, M. D. Santis, L. D. Stasio, P. Varilone, and P. Verde, "Detecting the origin of the voltage sags measured in the smart grids," in *Proc. Int. Conf. Clean Electr. Power (ICCEP)*, Jul. 2019, pp. 129–135.
[41] K. Skaloumpakas, J. C. Boemer, E. van Ruitenbeek, M. Gibescu, and M. A. M. M. van der Meijden, "Response of low voltage networks with high penetration of photovoltaic systems to transmission network faults," in *Proc. 3rd Renew. Power Gener. Conf. (RPG)*, 2014, pp. 8–27.
[42] A. Safari, H. Shahsavari, and J. Salehi, "A mathematical model of SOFC power plant for dynamic simulation of multi-machine power systems," *Energy*, vol. 149, pp. 397–413, Apr. 2018.
[43] Y. Mohamed and E. F. El-Saadany, "Adaptive decentralized droop controller to preserve power sharing stability of paralleled inverters in distributed generation microgrids," *IEEE Trans. Power Electron.*, vol. 23, no. 6, pp. 2806–2816, Nov. 2008.
[44] Y. Hu, X. Wang, Y. Peng, J. Xiang, and W. Wei, "Distributed finite-time secondary control for DC microgrids with virtual impedance arrangement," *IEEE Access*, vol. 7, pp. 57060–57068, 2019.
[45] W. Dong, H. Xin, D. Wu, and L. Huang, "Small signal stability analysis of multi-infeed power electronic systems based on grid strength assessment," *IEEE Trans. Power Syst.*, vol. 34, no. 2, pp. 1393–1403, Mar. 2019.
[46] F. Milano, "Semi-implicit formulation of differential-algebraic equations for transient stability analysis," *IEEE Trans. Power Syst.*, vol. 31, no. 6, pp. 4534–4543, Nov. 2016.
[47] Y. Zhou and V. Ajjarapu, "A novel approach to trace time-domain trajectories of power systems in multiple time scales," *IEEE Trans. Power Syst.*, vol. 20, no. 1, pp. 149–155, Feb. 2005.
[48] Y. Liu and K. Sun, "Solving power system differential algebraic equations using differential transformation," *IEEE Trans. Power Syst.*, vol. 35, no. 3, pp. 2289–2299, May 2020.
[49] Z. Tian, W. Wu, and B. Zhang, "A mixed integer quadratic programming model for topology identification in distribution network," *IEEE Trans. Power Syst.*, vol. 31, no. 1, pp. 823–824, Jan. 2016.
[50] A. Bidram, A. Davoudi, F. L. Lewis, and S. Sam Ge, "Distributed adaptive voltage control of inverter-based microgrids," *IEEE Trans. Energy Convers.*, vol. 29, no. 4, pp. 862–872, Dec. 2014.
[51] S. Mishra and D. Ramasubramanian, "Distributed adaptive voltage control of inverter-based microgrids," *IEEE Trans. Power Syst.*, vol. 30, no. 1, pp. 166–176, Jan. 2015.
[52] I. A. Quadri, S. Bhowmick, and D. Joshi, "A comprehensive technique for optimal allocation of distributed energy resources in radial distribution systems," *Appl. Energy*, vol. 211, pp. 1245–1260, Feb. 2018.

POUYA SALYANI received the B.Sc. and M.Sc. degrees in power electrical engineering from Azarbaijan Shahid Madani University, Tabriz, Iran, in 2015 and 2018, respectively. He is currently pursuing the Ph.D. degree in power electrical engineering with the University of Tabriz, Iran. His research interests include distribution networks, power system optimization, low-voltage ride through assessment, planning of distribution networks, reliability, demand response, and energy markets.

KAZEM ZARE received the B.Sc. and M.Sc. degrees in electrical engineering from the University of Tabriz, Tabriz, Iran, in 2000 and 2003, respectively, and the Ph.D. degree from Tarbiat Modares University, Tehran, Iran, in 2009.

He is currently a Professor with the Faculty of Electrical and Computer Engineering, University of Tabriz. His research interests include power system economics, distribution networks, microgrid, energy management, smart building, demand response, and power system optimization.

MEHDI ABAPOUR (Member, IEEE) received the B.Sc. and M.Sc. degrees in electrical engineering from the University of Tabriz, Tabriz, Iran, in 2005 and 2007, respectively, and the Ph.D. degree in electrical engineering from Tarbiat Modares University, Tehran, Iran, in 2013. He is currently an Associate Professor with the School of Electrical and Computer Engineering, University of Tabriz. His research interests include reliability, energy management, demand response, and power electronics.

AMIN SAFARI received the B.Sc. degree in electrical engineering from the University of Tabriz, in 2007, the M.Sc. degree in electrical engineering from the University of Zanjan, in 2009, and the Ph.D. degree in electrical engineering from the Iran University of Science and Technology, Iran, in 2013. He is currently an Associate Professor with the Department of Electrical Engineering, Azarbaijan Shahid Madani University, Tabriz, Iran. His research interests include application of artificial intelligence, heuristic optimization algorithms to power system design, FACTS device, power system analysis and control, renewable energy, control and management of microgrids, and smart grid.

MIADREZA SHAFIE-KHAH (Senior Member, IEEE) received the M.Sc. and Ph.D. degrees in electrical engineering from Tarbiat Modares University, Tehran, Iran, in 2008 and 2012, respectively, the Ph.D. degree from the University of Beira Interior (UBI), Covilha, Portugal, in 2015, and the Ph.D. degree from the University of Salerno, Salerno, Italy, in 2016. He is currently a tenure-track Professor with the University of Vaasa, Vaasa, Finland. His research interests include power market simulation, market power monitoring, power system optimization, demand response, electric vehicles, price forecasting, and smart grids. He serves as an Associate Editor for *IET-RPG*. He also serves as an Editor for the IEEE Open Access Journal of Power and Energy. He was one of the Outstanding Reviewers of the IEEE Transactions on Sustainable Energy, in 2014 and 2017, one of the Best Reviewers of the IEEE Transactions on Smart Grid, in 2016 and 2017, and one of the Outstanding Reviewers of the IEEE Transactions on Power Systems, in 2017 and 2018.